Progress In Electromagnetics Research B, Vol. 73, 31–48, 2017

Design, Analysis and Implementation of Ultra High Data Rate UWB Six-Port Receiver up to 7 Gbps for 5G New Spectrum Radio Access and CAR

Gholamreza Askari* **and Mahmoud Kamarei**

Abstract—Every generation of mobile communication has been associated with higher data rates than the previous generation. So 5G new spectrum radio access should support data rates exceeding 10 Gbps in most of its applications. An Ultra Wide Band (UWB) ultrahigh data rate full six-port receiver architecture up to 6.7 Gbps for 5G new spectrum is presented in this paper. The proposed structure is constructed using one UWB ultra-high data rate Wilkinson power divider/combiner and three UWB ultra-high data rate two-stage branch line couplers which are the essential components of any full six-port structure. The design procedure, optimization and implementation of these two UWB essential components in 21–30 GHz are completely done to achieve the optimum performance of final six-port structure. The final fabrication results show the average of −14 dB of input matching, −20 dB of isolation of isolated Ports, −4.2 dB of coupling in output ports (considering 2 SMA connectors and transitions in each path), and linear phase variation of outputs in the whole bandwidth of 21–30 GHz. To analyze and qualify the UWB six-port structure in any specific application in 5G and other UWB high data rate applications, a new analytical formulation with a new six-port structure of non-ideal UWB six-port circuit is presented. With this new analytical model and new configuration, there is no need to calibrate the outputs of in-phase and quad phase of the six-port receiver outputs. Based on the final fabricated essential components and the new analytical model, the final full six-port structure is constructed and analysed using UWB-OFDM with QPSK and 16QAM demodulation schemes in its sub-bands. To complete and verify the new analysis and to validate the final constructed UWB six-port structure and its essential components in ultra-high data rate application in 5G new spectrum, the UWB-IR impulse radio with modulated ultra-high data rate signal up to 7 Gbps and in 21–30 GHz bandwidth is completely discussed. The results show that all clusters of demodulated constellations are very well positioned and individualized in whole bandwidth in all modulation schemes. Also this new design and configuration of six-port receiver improves the dynamic range of the RF input signals up to 60 dB which is valuable. During the design procedure, a very useful method to choose the suitable laminate based on the time, frequency and two dimensional Wigner-Vile Distribution methods is presented. Also, some practical issues in design and implementation of the UWB microstrip component such as transitions are considered to achieve the best results.

1. INTRODUCTION

Ultra-high speed connections in the range of multi-gigabit per second (up to 10 Gbps) could potentially be achieved through using ultra-wide carrier bandwidths in the order of up to several hundred MHz or multi-GHz. Many proposed applications in 5G need ultra-high speed links and data rates, such as UHD video (4 k, 8 k), virtual reality, vehicles (cars, buses, trains, aerial stations, etc.), and collision avoidance

Received 16 September 2016, Accepted 8 February 2017, Scheduled 23 February 2017

* Corresponding author: Gholamreza Askari (askarigh@ut.ac.ir).

The authors are with the School of Electrical and Computer Engineering, University College of Engineering, University of Tehran, North Kargar st., Tehran, Iran.

Radar (CAR). There are significant studies underway in both industry and academia on characterization of frequencies below and above 30 GHz for 5G applications. Penetration loss, diffraction loss, etc., also increase, with increasing frequency, so the bands between 6–30 GHz are important to consider due to propagation reasons [1, 2]. Also for automotive UWB short range radar systems, the FCC allocated the band 22–29 GHz. The new decision permits the use of radar frequencies in this band until 2018, with a phase out for existing CAR lines until 2022 [3].

On the other hand, modern wireless sensing and communication systems are often based on high bandwidth and high carrier frequencies. In the range beyond 100 GHz, low-cost communication direct-receivers which are less complex and allow a higher integration level than conventional heterodyne receivers are needed. High bandwidth is an important problem for these systems [4, 5]. Also many microwave applications require the determination of a ratio of two complex voltages or two complex wave amplitudes over a specified frequency band [6]. In these contexts, a six-port receiver is a good alternative, as well as for low volume markets. Six-port technology has been under development over past 30 years, and this concept is a serious alternative for microwave and millimeter-wave frequencies and ultrahigh-bandwidth applications in wireless sensing, radar, medical and communication systems [4–8]. Good matching at all ports, good isolation between ports, good phase and amplitude balance, within the desired frequency band are the main goals in design procedure. These design requirements and also the non-idealities of the six-port network can be understood by the analysis of the six-port scattering (S-) matrix. There are some analytical or simulation/measurement six-port analysis in literatures, but some of them considered an ideal narrow band six-port [S]-matrix, and some of them are only dependent on simulation or measurement results [9–15].

A six-port vector voltmeter or six-port modulator/demodulator can be designed using three 3-dB quadrature couplers and one in-phase or out-of-phase power divider which are the essential components of the six-port structure. Several circuits as rat-race, hybrid coupler, and T-junction are key components in the design of microwave devices, due to their planar integration, wide bandwidth in power dividing distribution, and high isolation factor between requested ports [14, 6]. However, many of them are not appropriate in near millimeter wave applications because of fabrication difficulty and other challenges. Moreover, applying the available designs of UWB couplers and dividers, from the open microwave literature, is also a challenge [6], and several technologies have been intensively used for the millimeter wave circuit design and in house prototype fabrication as coplanar, Substrate Integrated Waveguide (SIW), and microstrip technology. The coplanar technology assures high-quality component design, but it is not well suited for low-cost production due to the difficulties in automating wire-bonding implementation, necessary for obtaining repeatable performances. On the other hand, the SIW technology assures high-quality component design on thin ceramics or the design of optimal transitions from planar to standard rectangular waveguides. For further circuit miniaturization, the microstrip technology on a suitable substrate is recommended [15, 16]. But choosing suitable laminates for the design and implementation of UWB short pulse signals is a main challenge [16, 17].

In this paper, design procedure, analysis and implementation of an Ultra Wide Band (UWB) ultrahigh data rate full six-port receiver architecture up to 6.7 Gbps in 21–30 GHz is presented. In section 2, first a very useful method to choose the suitable laminate based on the time, frequency and two-dimensional Wigner-Vile distribution methods is presented. Then the design procedure, optimization and implementation of two UWB Wilkinson power dividers/combiners and UWB two-stage branch line couplers which are the essential components of the final six-port structure in 21–30 GHz are discussed and done. After that in section three, a new analytical model and configuration of non-ideal UWB six-port networks is presented. Then based on the final fabricated essential components and the new analytical model, the final full six-port structure is constructed and analysed using UWB-OFDM with QPSK and 16QAM demodulation schemes in its sub-bands and the UWB-IR impulse radio with modulated ultra-high data rate signal up to 7 Gbps in 21–30 GHz bandwidth. Finally the paper is concluded in section four.

2. DESIGN PROCEDURE

The six-port circuit is in fact an RF six-port interferometer with a variety of architectures consisting power dividers, couplers, and phase shifters. These RF components are interconnected in such a way

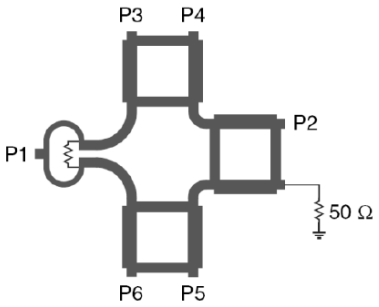

Figure 1. Layout of the full six-port components.

that four different vector sums of the reference signal and signal to be directly measured (or up/down-converted) are produced [8]. After processing two signals in the radio-frequency (RF) domain, the results are down converted to baseband. The six-port structure has two input ports and four output ports. The processing is carried out by a superposition of the two input signals with four different relative phases. For the six-port architecture, the total phase of one full-wave period (2π) is divided into four parts shifted by $\pi/2$, respectively. Therefore, the relative phase differences between the two input signals are 0, $\pi/2$, π, and $3\pi/2$. Here, the six-port structure, shown in Fig. 1, is considered by one 3-dB Wilkinson power divider and three 3-dB quadrature hybrid couplers.

As shown in Fig. 1, two essential components of the six-port structure are a 3-dB Wilkinson power divider and a 3-dB quadrature hybrid coupler. In this section, first a good method to choose the suitable laminate for UWB applications to minimize distortion along microstrip lines is presented. Then, design, optimization and implementation of two UWB essential components of the proposed six-port structure in 21–30 GHz are completely discussed to achieve the optimum performance of the final six-port structure, which is analyzed completely in the next section.

2.1. Suitable Laminates to Design and Implementation of Ultra Wideband Components

Two types of UWB signals are noticeable, UWB Gaussian pulse types and modulated Gaussian short pulse in microwave and mm-wave applications for ultra-fast communications, collision avoidance radars, etc. As explained before for an automotive UWB short range radar applications in this paper, the modulated UWB pulses with bandwidth of 21–30 GHz are considered. To have a great performance in UWB short pulse signals, all distortions in time and frequency domains must be negligible or removed. So the choices of the appropriate laminates for transmit/receive UWB waveforms and their propagation and minimum distortion in time and frequency domain of them across the circuit are very important. The most adapted waveforms for detection functionality of radar are the types of Gaussian pulses [18] which are considered in this work. In this section, based on the authors' analysis [16] and other design limitations such as six-port component constructions, RT/duroid 5880 with the relative permittivity about 2.2, copper thickness of 17 µm, roughness of 1.8 µm and dielectric loss tan. about 0.0023 with different substrate thicknesses of 5, 10 and 20 mil and 10 cm of length are studied in the UWB signals distortion analysis. The 10 cm lines of each laminate with different thicknesses and wave ports in the input and output are designed and optimized by the ADS software full-wave analysis of two types of UWB signals, respectively. Wave ports are considered because in this section the focus is on different laminate dispersion behaviours. Fig. 2 shows frequency domain responses of these microstrip lines.

By analyzing the procedure reported in [16], as shown in group delay part of Fig. 2, it can be seen that the minimum distortion in the phase or group delay of modulated UWB short pulse signal in 21–30 GHz is with 5 mil laminate. On the other hand, from the insertion loss curves in Fig. 2 it is seen that 5 mil laminate has more insertion loss and large variation in this band and may cause amplitude distortion in the modulated UWB signals. For more study, let's inject modulated Gaussian short pulse in these three optimized lines. This pulse has about 16 GHz 3 dB bandwidth and about 40 psec 10 dB pulse width. The output results are shown in Fig. 3.

As can be seen from Fig. 3, 5 mil laminates are not a good choice for this application. Also from

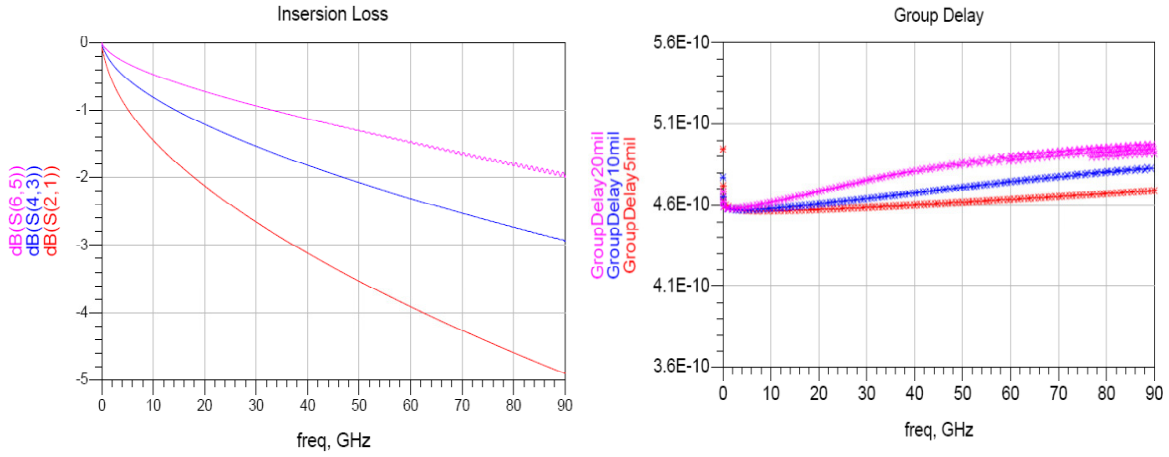

Figure 2. Insertion loss and group delay of 5 mil $(S2,1)$, 10 mil $(S4,3)$ and 20 mil $(S6,5)$ laminates.

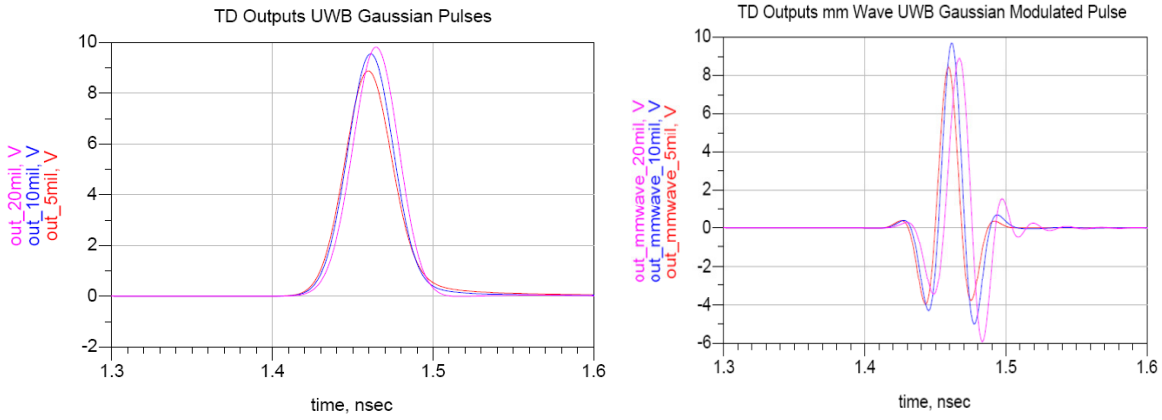

Figure 3. Output signals of the simple Gaussian and modulated Gaussian short pulses across 5, 10 and 20 mil laminates.

the different results of Fig. 2 and Fig. 3 it is difficult to choose 10 mil or 20 mil laminate, which adds detection and recognition of multi-object reflection and high-speed communication problems to these uncertainties. For this purpose, two-dimensional distributions or Time Frequency Distribution (TFD) not only can help in the analysis of time-frequency distortion, but also can analyze time-frequency characterization of the complex received signals. One of the best TFDs is the Wigner-Ville Distribution (WVD) which can be expressed by the following equation [16].

$$\rho_z(t,f) = W_z(t,f) = \int_{-\infty}^{\infty} z\left(t+\frac{\tau}{2}\right) z^*\left(t-\frac{\tau}{2}\right) e^{-j2\pi f\tau} d\tau$$

After discretization of the Wigner-Ville distribution and selection of suitable windowing for time and frequency variables, which is done in this paper, the output signals of Fig. 3 are considered to be analyzed with WVD. A MATLAB code was prepared for this purpose. Fig. 4 shows the WVD of the propagated modulated UWB Gaussian pulses across the optimized 10 cm lines with 10 mil and 20 mil thicknesses. As can be seen from this figure, the output results of the 10 mil laminate is more concentrated in a limited bandwidth and time, and some multi dominant components in the results of the 20 mil laminate are outspread and insufficient. Furthermore, other limitations such as realization design and input-output transitions, which are considered in this paper and previous work of the authors [19], must be perceived. So the 10 mil laminate of RT/duroid 5880 with the relative permittivity about 2.2, copper thickness of 17 µm, roughness of 1.8 µm and dielectric loss tan. about 0.0023 is selected in this paper to design the six-port structure.

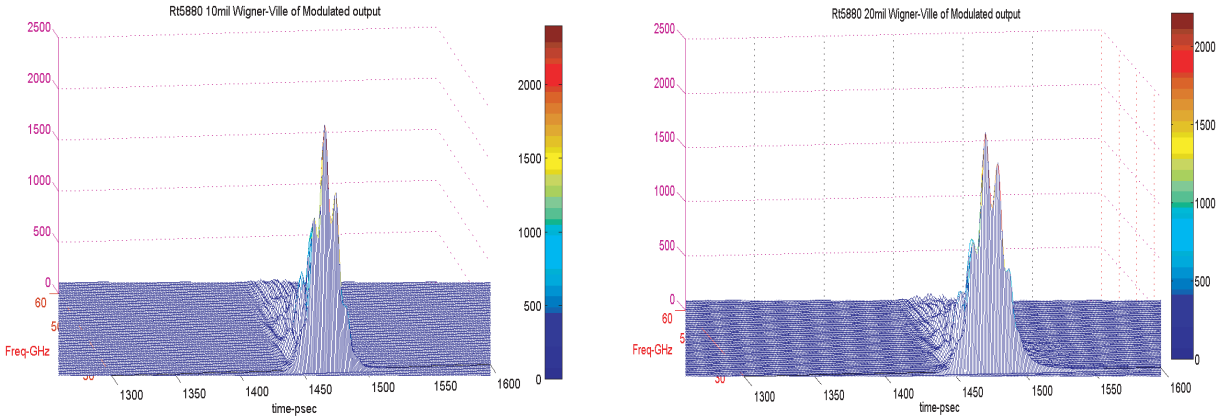

(a) (b)

Figure 4. WVD of the propagated UWB modulated Gaussian pulses across the (a) 10 mil and (b) 20 mil laminates.

2.2. UWB Wilkinson Power Divider

The most widely known power dividers/combiners are the Wilkinson power divider. However, at near millimeter wave frequencies, the two output arms of the conventional Wilkinson circuit must be placed very close to each other, to be connected to the 100 Ω resistor. This layout raises undesirable mutual coupling between the output lines. To design a Wilkinson power divider for millimeter wave applications, it is necessary to modify the traditional Wilkinson to connect the integrated resistor. So the additional transmission lines can be a good candidate to create an ideal layout for this isolation resistor [14]. These additional lines create an ideal framework for this isolation resistor, reducing undesirable mutual coupling between the transformer arms. The layout of this power divider is depicted in Fig. 5.

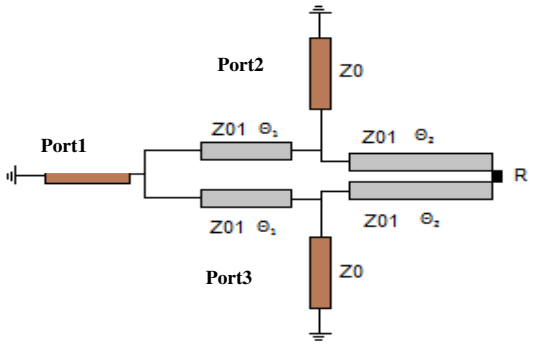

Figure 5. Proposed modified Wilkinson power divider.

As shown in Fig. 5, the line of symmetry bisects the resistor in two series resistors of $R/2$, doubling the effective impedance of input port 1. All impedances are normalized to Z_o. As formulated in [14], there are four unknown parameters; the characteristic impedance of Z_{01}, electrical lengths θ_1 and θ_2, and resistor R which should be determined for the desired frequency bandwidth. Several equations can be obtained by using even and odd mode analysis method [14, 20]. In this analysis, it is possible to depict the Wilkinson power divider circuit in the normalized and symmetric form. For even-mode excitation, no current flows through resistors, or the even mode analysis gives a virtual open circuit along the symmetry line, eliminating the resistor R. So it can be considered a two-port circuit for even

mode analysis with the normalized $ABCD$ matrix of Eq. (1)

$$\begin{bmatrix} A_e & B_e \\ C_e & D_e \end{bmatrix} = \begin{bmatrix} 1 & 0 \\ \dfrac{j\tan\theta_2}{Z_{01}} & 1 \end{bmatrix} \begin{bmatrix} \cos\theta_1 & jZ_{01}\sin\theta_1 \\ \dfrac{j\sin\theta_1}{Z_{01}} & \cos\theta_1 \end{bmatrix}. \tag{1}$$

It is noted that matching and isolation conditions related to ports 2 and 3 yield $S_{22e} = S_{22o} = 0$. So imposing the real and imaginary parts of the even return loss S_{22e} equal to zero yields Eq. (2).

$$\tan\theta_1 = -\frac{1}{\tan\theta_2}, \quad 1 - \frac{z_{01}^2}{2} = \frac{1}{(\tan\theta_1)^2}, \quad \text{where } z_{01} = \frac{Z_{01}}{Z_0}, \tag{2}$$

In the odd mode analysis, the symmetry line corresponds to a virtual short circuit, eliminating port 1. Therefore, the odd return loss is calculated using the impedance of the resulting mono-port. So Equation (3) is obtained by equaling the real and imaginary parts of S_{22o} to zero

$$1 - \frac{r}{2} = \frac{1}{(\tan\theta_1)^2} \quad r = z_{01}^2 \tag{3}$$

r is the normalized resistor. According to Equation (2), $\theta 1$ and θ_2 must be orthogonal. r is selected equal to 2 which is a particular solution of Eqs. (2) and (3). The corresponding electric lengths θ_1 and θ_2 are $\pi/2$ and π, respectively, and the normalized ring characteristic impedance z_{01} is $\sqrt{2}$.

According to the above process, the Wilkinson divider is designed at center frequency of 26 GHz using ADS and CST softwares. We got respectively -15 dB and -20 dB of matching and isolation of input ports and -4 dB of coupling (considering 2 SMA connectors and transitions) between input-output ports as shown in Fig. 6.

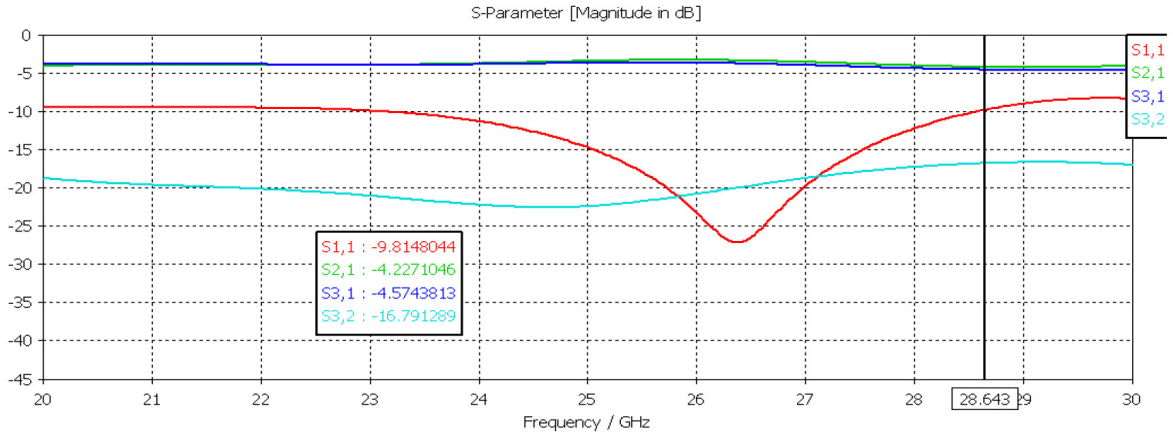

Figure 6. Simulation results of magnitude of S parameters of designed Wilkinson divider.

A coaxial-to-microstrip transition is required to improve the performance of Wilkinson divider. The coaxial-to-microstrip transition must support only a single propagating mode over a broad frequency, and it is important to be simple, low-cost and wideband. The authors presented a useful wideband coaxial-to-microstrip transition in [19]. The first consideration in design of transition is impedance matching, so the coaxial and microstrip lines are designed to be 50 Ω. But having the same characteristic impedance does not always guarantee a good transition between two transmission lines, and the field distributions of the transmission line must be also matched. Center conductor of SMA is wider than microstrip line, and therefore, direct soldering of them causes an impedance mismatch, so a conductor backed CPW (CB-CPW) pre-transition section is used to ensure proper field match between coaxial and microstrip lines. The transition and total geometry are shown in Fig. 7. The parameters of the transition are $W1 = 0.78$; $W2 = 1.4137$; $D1 = 1.6$; $D2 = 0.7$; $G1 = 0.396$; $L1 = 2.154$ and $dx = 0.7$ (all in millimeter). In the CB-CPW section, the values of $W1$ and $G1$ are chosen in order to yield a characteristic impedance of 50 ohm along the transition within the desired frequency band. The value

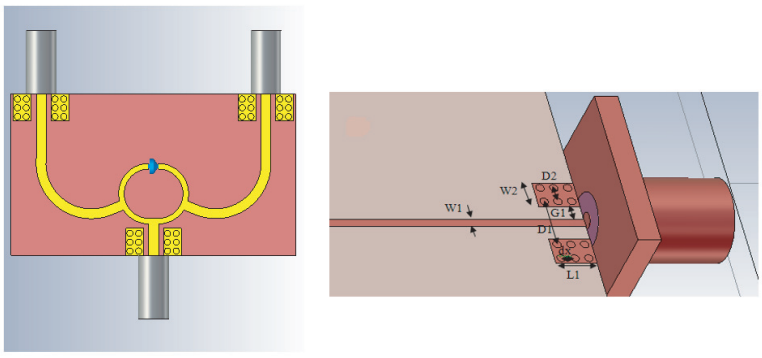

(a) (b)

Figure 7. (a) The CST model of proposed modified Wilkinson. (b) The proposed transition.

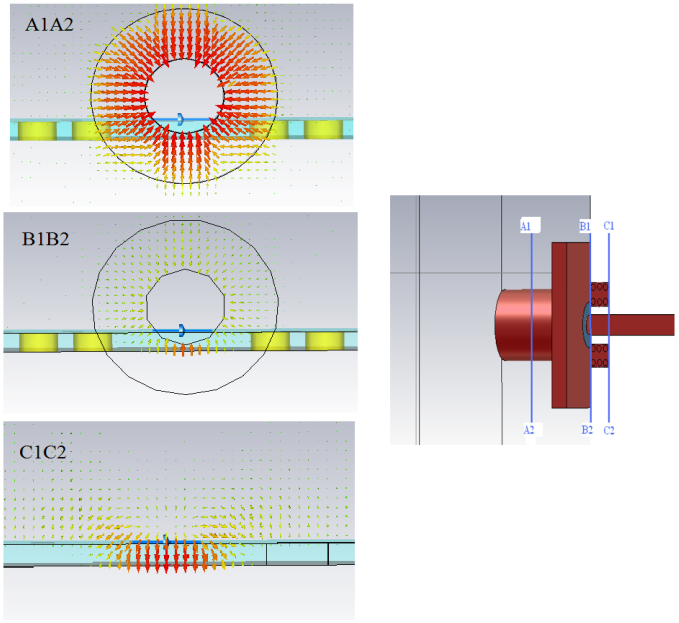

Figure 8. Magnitude and direction of the electric field from top to down: A1A2: center of the coaxial connector, B1B2: coaxial to GCPW contact, and C1C2: GCPW to Microstrip contact.

of $W1$ is chosen nearly equal to the width of microstrip line to avoid any abrupt discontinuity and to minimize the reflection along the transition. In this transition, the number of vias and placement of them are optimized to suppress parallel plate mode and radiation loss and to obtain maximum bandwidth. The electromagnetic fields of the transition structures are shown in Fig. 8 which is analyzed with CST.

S parameters of the modified Wilkinson with the proposed transition are shown in Fig. 9. The bandwidth of power divider is 21–30 GHz with less than 0.2 dB ripple of transmission coefficient. Comparing the Fig. 6 and Fig. 9, it is clear that all S-parameters of the new Wilkinson divider with proposed transition are better than the previous ones.

The final designed Wilkinson power divider with the proposed transition is implemented on an RT/Duroid 5880 Rogers laminate and using two 2.4 mm SMA air coaxial connectors as depicted in Fig. 10. The measured results are extracted using the Network Analyzer model hp 8510C which are shown in Fig. 11. As shown in this figure, the average of -13 dB of input matching and -20 dB of isolation of output ports and the average of -4.2 dB of coupling between input-output ports (considering 2 SMA connectors and transitions) in the bandwidth of 21–30 GHz are achieved with the proposed Wilkinson power divider.

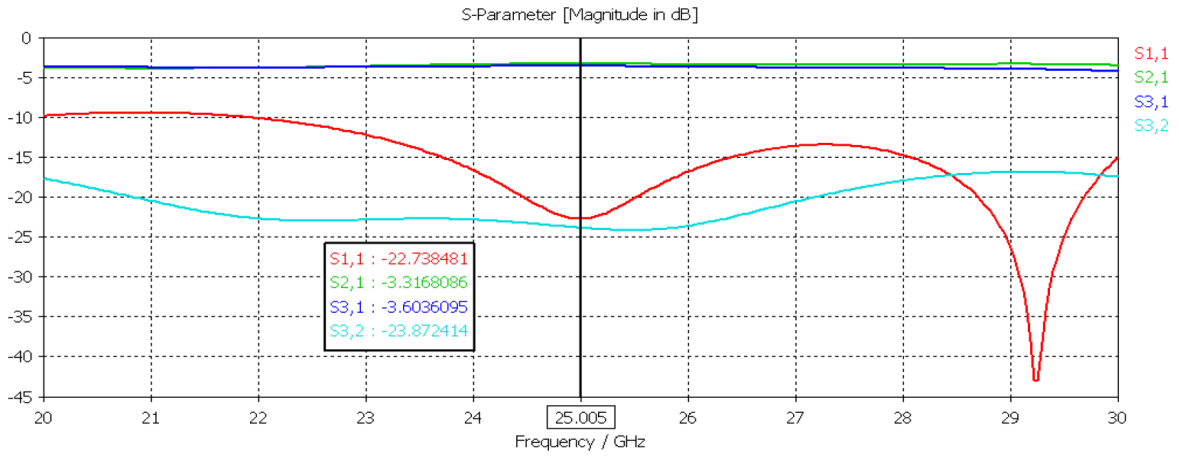

Figure 9. Simulation results of magnitude of S parameters of new Wilkinson divider with transition.

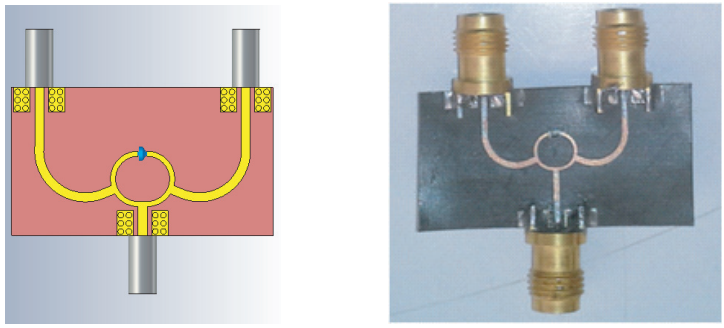

(a) (b)

Figure 10. (a) The CST model of the proposed modified Wilkinson. (b) The implemented photo of the proposed modified Wilkinson.

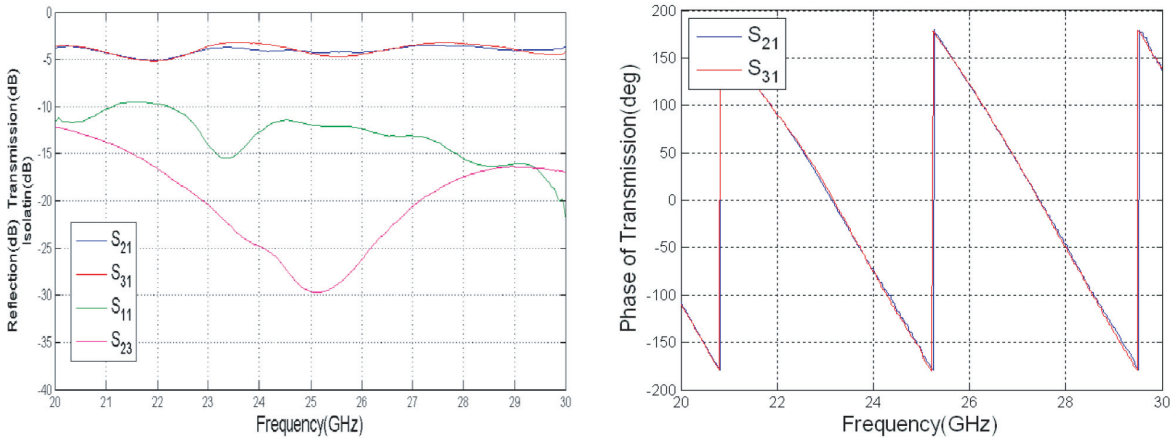

(a) (b)

Figure 11. The measured S parameters results of the proposed Wilkinson; (a) Amplitude of the input reflection ($S11$), transmissions ($S21$, $S31$), and isolation ($S23$) and (b) phase of the transmission coefficients.

2.3. UWB Quadrature Branch Line Coupler

Branch line couplers offer a 90° phase difference with good directivity and equal/unequal power splitting which is useful in a large number of RFs, microwave and mm-wave circuits such as balanced mixer, phase

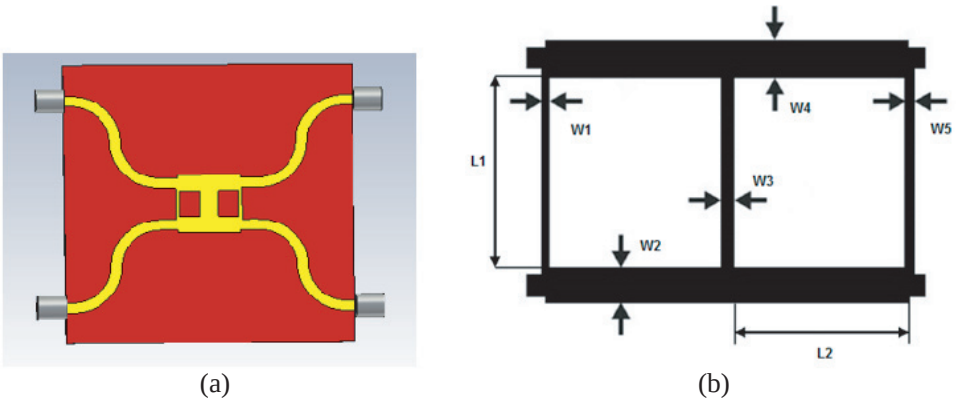

Figure 12. (a) The CST model of proposed branch line coupler, (b) ADS model.

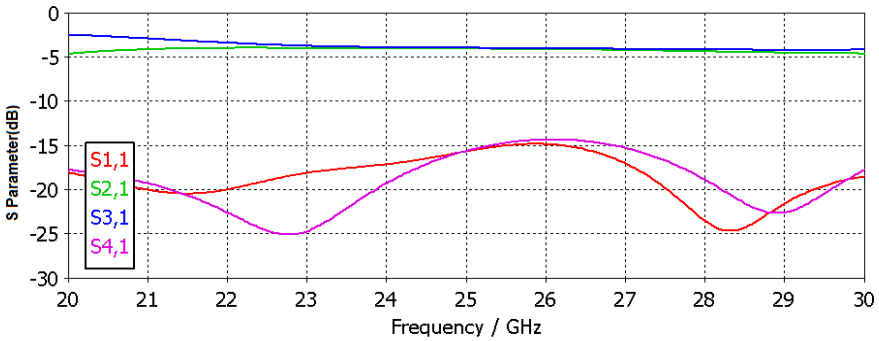

Figure 13. Simulation results of magnitude of proposed branch line coupler.

correlator, balanced amplifier, image rejection mixer, balanced modulator, programmable attenuator, power measurements, antenna beam forming networks and other microwave instrumentations. A single-section branch line coupler with equal power division is the most popular structure, but due to the quarter wavelength requirement, its bandwidth is limited to 10%. The bandwidth can be improved to a decade or more by using multiple sections in cascade. There are many circuits that can be used as broadband 90° hybrids such as Lange coupler and coupled line couplers. But Lange coupler involves realization of very narrow lines and spacing apart from wire bonding. Also 3-dB couplers in edge coupled microstrip configuration are impossible to realize as the coupled line spacing is only a few microns. Couplers using offset coupled strip lines involve multiple layers, hence not suitable for one layer applications. Most of the 3-dB couplers require multi-layered or air-bridged structures for tight coupling and signal routing (crossover) over a wide frequency range. The requirements for air-bridges result in more masks and fabrication processes leading to more manufacturing costs. Moreover, these air-bridges would represent a bottleneck for power handling, which limits the applications of Lange and tandem couplers [21]. The best feasible technique to enhance the bandwidth is using a multi-section cascaded branch line coupler. In this section, a compact, UWB 2-section 3-dB branch line coupler is designed and implemented in 21–30 GHz in microstrip technology using Ansoft Designer and CST softwares based full EM simulation. At first, the schematic circuit is created using ideal components. Next, the impedance values of the ideal transmission lines are synthesized to specify the length and width values of microstrip lines on the chosen substrate. After that, the imbalance and isolation conditions of the coupler are optimized in ADS software, and finally, considering input and output connectors and transitions, the UWB 2-section 3-dB branch line coupler is optimized in CST software. The minimum line width is chosen 0.2 mm for fabrication limits. Furthermore, the ideal width should not exceed $\lambda/8$ at the top frequency. The final geometrical parameters are $L1 = 2\,\text{mm}$, $L2 = 1.5\,\text{mm}$, $W1 = 0.25$, $W2 = 1.2601$, $W3 = 1.3002$, $W4 = 1.2601$, $W5 = 1.2601$ (Fig. 12). The simulation results are shown in Fig. 13.

The final designed 2-section branch line coupler is implemented on an RT/Duroid 5880 Rogers laminate using two 2.4 mm SMA air coaxial connectors as depicted in Fig. 15. The measured results are extracted using the Network Analyzer model hp 8510C, shown in Fig. 14. As shown in this figure, the average of −15 dB of input matching and −20 dB of isolation of isolated ports and the average of −4.3 dB of coupling between input-output ports (considering 2 SMA connectors and transitions) in the total bandwidth of 21–30 GHz are achieved with the proposed 2-section branch line coupler. Fig. 15 shows photos of the fabricated hybrid and the measurements test setup.

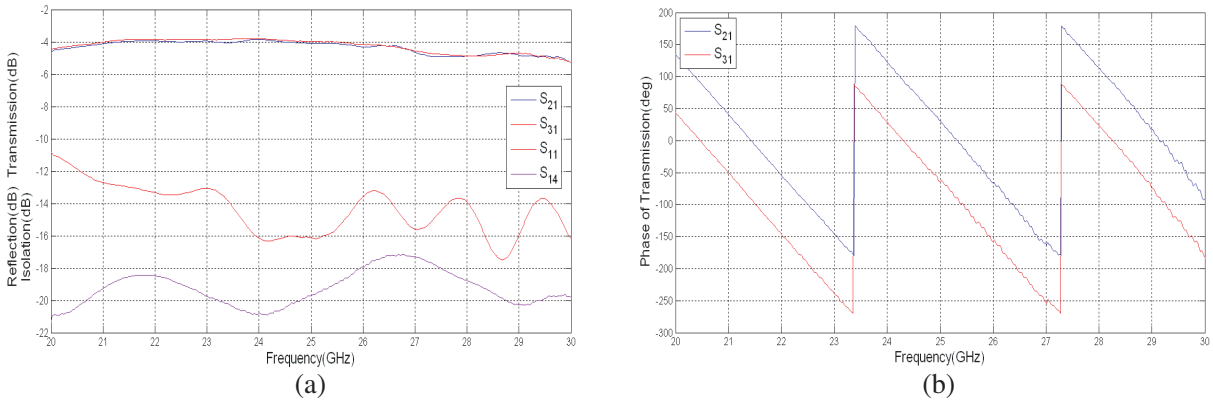

(a) (b)

Figure 14. The measured S parameters of the proposed hybrid; (a) Amplitude of the input reflection ($S11$), transmissions ($S21$, $S31$), and isolation ($S14$) and (b) phase of the transmission coefficients.

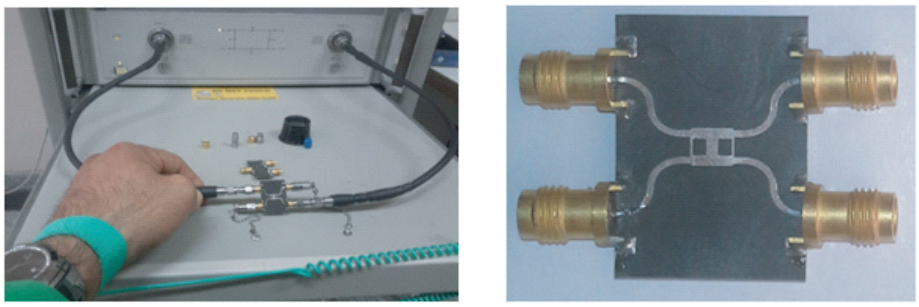

(a) (b)

Figure 15. (a) The measurement setup of the proposed Wilkinson and branch line coupler. (b) Fabricated coupler.

3. FULL PORT ANALYSIS

3.1. The Narrow Band Six-Port Demodulator

Regardless of which view of the six-port receiver/transmitter is chosen, the wireless sensing or communications setup, the basic principle is the same. A complete theory, validated by various simulations and measurements of direct conversion receivers, has been published in recent years [8–15]. A schematic of six-port structure is shown in Fig. 16. The local oscillator (LO) signal of frequency ω_{LO} is applied to port 1 of the six-port network, and the received RF modulated signal is applied to port 4 with carrier frequency of ωc. As shown in Fig. 16, matched pairs of zero-biased Schottky diode power detectors provide mixing function by squaring the signals at ports 3, 4, 5 and 6. After the diodes, high frequencies terms are filtered by LPF and the I and Q-signals are obtained by means of two differential amplifiers.

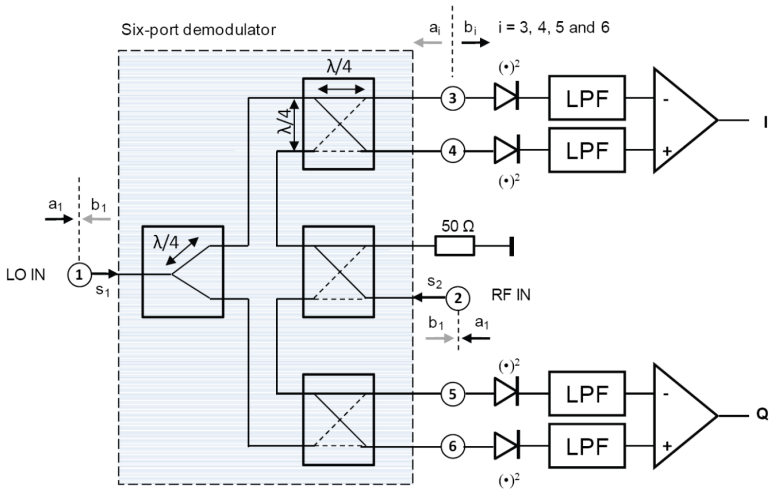

Figure 16. Schematic of the six-port demodulator.

The ideal $[S]$ parameters scattering matrix of the proposed six-port structure can be obtained as,

$$[S] = \frac{1}{2}\begin{bmatrix} 0 & 0 & e^{-j180} & e^{-j270} & e^{-j270} & e^{-j180} \\ 0 & 0 & e^{-j0} & e^{-j270} & e^{-j180} & e^{-j270} \\ e^{-j180} & e^{-j0} & 0 & 0 & 0 & 0 \\ e^{-j270} & e^{-j270} & 0 & 0 & 0 & 0 \\ e^{-j270} & e^{-j180} & 0 & 0 & 0 & 0 \\ e^{-j180} & e^{-j270} & 0 & 0 & 0 & 0 \end{bmatrix} \tag{4}$$

By using the $[S]$ parameters scattering matrix of the components, we can get the signal values equations for the four output ports as the following:

$$b_3 = 1/2(-a_1 + a_2); \quad b_4 = 1/2(ja_1 + ja_2); \quad b_5 = 1/2(ja_1 - a_2); \quad b_6 = 1/2(-a_1 + ja_2) \tag{5}$$

Assume that the inputs LO signal and RF modulated signal in time domain are:

$$\begin{aligned} s_1 &= s_{\mathrm{LO}}(t) = A_{\mathrm{LO}} \cos \omega_{\mathrm{LO}} t, \\ s_4 &= s_{\mathrm{RF}}(t) = A_{\mathrm{RF}}(t) \cos\left[\omega_c t + \phi_{\mathrm{RF}}(t)\right]. \end{aligned} \tag{6}$$

Using the methodology based on the S-parameters given by Eq. (4) of the six-port network, we can obtain the desired I and Q baseband signals as explained in [13]:

$$\begin{aligned} s_I(t) &= s_{3-2}(t) = A_{\mathrm{LO}} A_{\mathrm{RF}}(t) \cos\left[\phi_{\mathrm{RF}}(t)\right], \\ s_Q(t) &= s_{6-5}(t) = A_{\mathrm{LO}} A_{\mathrm{RF}}(t) \sin\left[\phi_{\mathrm{RF}}(t)\right]. \end{aligned} \tag{7}$$

3.2. New Non-Ideal UWB Six-Port Analysis

Considering a non-ideal $[S]$-matrix, a new real six-port network analysis in UWB is discussed in this section. In a non-ideal form of Fig. 16, in a complete analysis of the six-port structure, all 36 elements of the $6 * 6$ matrix should be considered, including the matched port. But 36 elements can make the analysis difficult, so some useful assumptions are considered to simplify the analysis, which are reciprocity, lossless, physical symmetry and simulation or measurement considerations.

Considering all above assumptions, all ideal narrow-band equations in previous section must be rewritten. So from Fig. 16, the outputs of ports 3–6 are:

$$\begin{aligned} b_3 &= |s(3,1)|\, A_{\mathrm{Lo}} \cos(\omega_{\mathrm{Lo}} t + \mathrm{phase}(s(3,1))) + |s(3,2)|\, A_{\mathrm{RF}} \cos(\omega_c t + \varphi_{\mathrm{RF}} + \mathrm{phase}(s(3,2))) \\ b_4 &= |s(4,1)|\, A_{\mathrm{Lo}} \cos(\omega_{\mathrm{Lo}} t + \mathrm{phase}(s(4,1))) + |s(4,2)|\, A_{\mathrm{RF}} \cos(\omega_c t + \varphi_{\mathrm{RF}} + \mathrm{phase}(s(4,2))) \\ \text{and also}: \; b_5 &= |s(5,1)| \ldots; \; b_6 = |s(6,1) \ldots| \end{aligned} \tag{8}$$

After passing through the six-port network, the signals at ports 3 to 6 in Eq. (8) are processed by zero-bias diodes. Again neglecting the dc component in the Taylor series describing the nonlinear operation of the diode, squaring operation in Eq. (8) and following low-pass filtering (LP) of the high-frequency components at $2f_{\mathrm{LO}}$, $2f_{\mathrm{RF}}$ and $f_{\mathrm{LO}} + f_{\mathrm{RF}}$ yield::

$$\begin{aligned} d_3 =& (|s(3,1)|\, A_{\mathrm{Lo}})^2 \Big/ 2 + (|s(3,2)|\, A_{\mathrm{RF}})^2 \Big/ 2 \\ &+ |s(3,1)|\, |s(3,2)| \times A_{\mathrm{Lo}} A_{\mathrm{RF}} \cos(\varphi_{\mathrm{RF}} + \mathrm{phase}(s(3,2)) - \mathrm{phase}(s(3,1))) \\ d_4 =& (|s(4,1)|\, A_{\mathrm{Lo}})^2 \Big/ 2 + (|s(4,2)|\, A_{\mathrm{RF}})^2 \Big/ 2 \\ &+ |s(4,1)|\, |s(4,2)| \times A_{\mathrm{Lo}} A_{\mathrm{RF}} \cos(\varphi_{\mathrm{RF}} + \mathrm{phase}(s(4,2)) - \mathrm{phase}(s(4,1))) \end{aligned} \tag{9}$$

and also: $d_5 = (\,|s(5,1)|\, A_{\mathrm{Lo}})^2 \Big/ 2 + \ldots ; d_6 = \ldots$

In-phase and quad-phase outputs are achieved by using two differential amplifiers and assuming $\omega_{\mathrm{Lo}} = \omega_c$.

$$I = d_4 - d_3 \qquad Q = d_6 - d_5 \tag{10}$$

$$\begin{aligned} I =& A_{\mathrm{Lo}}^2/2 \times \{|s(4,1)|^2 - |s(3,1)|^2\} + A_{\mathrm{RF}}^2/2 \times \{|s(4,2)|^2 - |s(3,2)|^2\} \\ &+ |s(4,1)|\, |s(4,2)|\, A_{\mathrm{Lo}} A_{\mathrm{RF}} \times \cos(\varphi_{\mathrm{RF}} + \mathrm{phase}(s(4,2)) - \mathrm{phase}(s(4,1))) \\ &- |s(3,1)|\, |s(3,2)|\, A_{\mathrm{Lo}} A_{\mathrm{RF}} \times \cos(\varphi_{\mathrm{RF}} + \mathrm{phase}(s(3,2)) - \mathrm{phase}(s(3,1))) \end{aligned} \tag{11}$$

and also: $$Q = A_{\mathrm{Lo}}^2/2 \times \{|s(6,1)|^2 - |s(5,1)|^2\} + A_{\mathrm{RF}}^2/2 \ldots \tag{12}$$

As can be seen from Eqs. (11) and (12), the formulations of Eq. (7) can be extracted with considering the ideal $[S]$-matrix in Eq. (4). Unlike the ideal narrow band, DC components are not removed from outputs I and Q, and the unsatisfied amplitude and phase in transmission coefficients over the frequency bandwidth can unbalance I and Q outputs. The first two terms of I and Q in Equations (11) and (12) are unwanted, and the first term which is the LO leakage is more important. It will be discussed in the next section that if these unwanted terms are not removed from I and Q outputs, the results are not satisfactory.

3.3. UWB Six-Port Construction

A novel six-port circuit, having an improved symmetry, has been designed using the novel Wilkinson power divider/combiner and the 90° hybrid couplers presented in previous sections. The central design frequency is 26 GHz, and the frequency bandwidth is 21–30 GHz. Fig. 17 shows the layout of the proposed six-port circuit composed of optimized elements and connected by 50 Ω coaxial connectors. The incident waves, RF input and reference LO (Local Oscillator) signals are applied to ports 1 and 4, respectively, and the output ports are 2, 3, 6 and 7. The simulation and optimization of the six-port structure are done using CST. As shown in Fig. 18, we get respectively −17 dB and −20 dB of matching

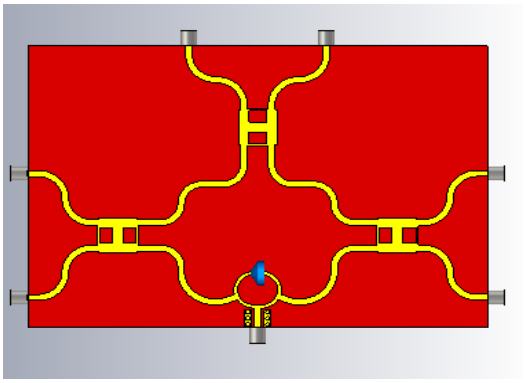

Figure 17. Layout of the new designed six-port coupler.

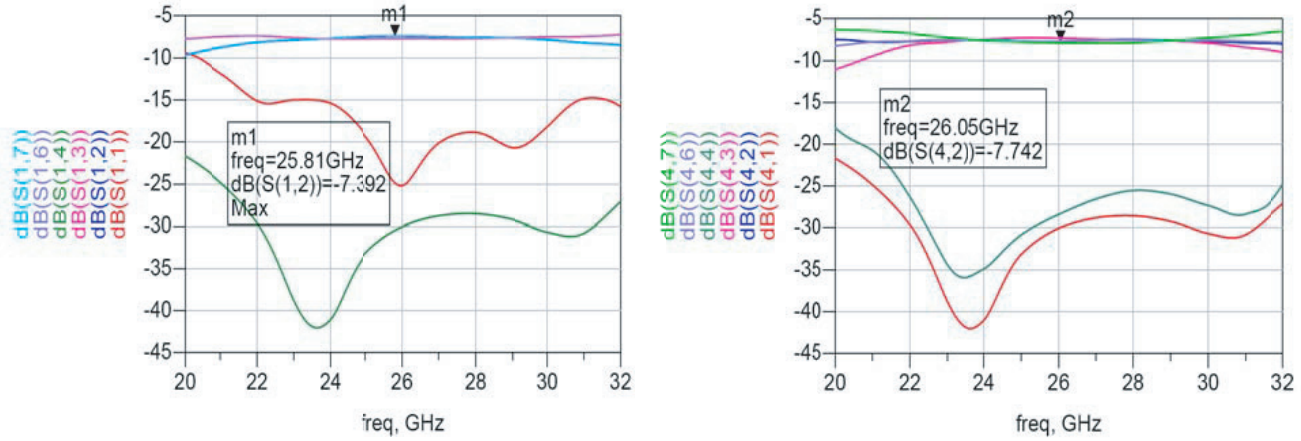

(a) (b)

Figure 18. The amplitude results of the transmission, reflection and isolation S parameters respect to the (a) LO port, (b) RF port.

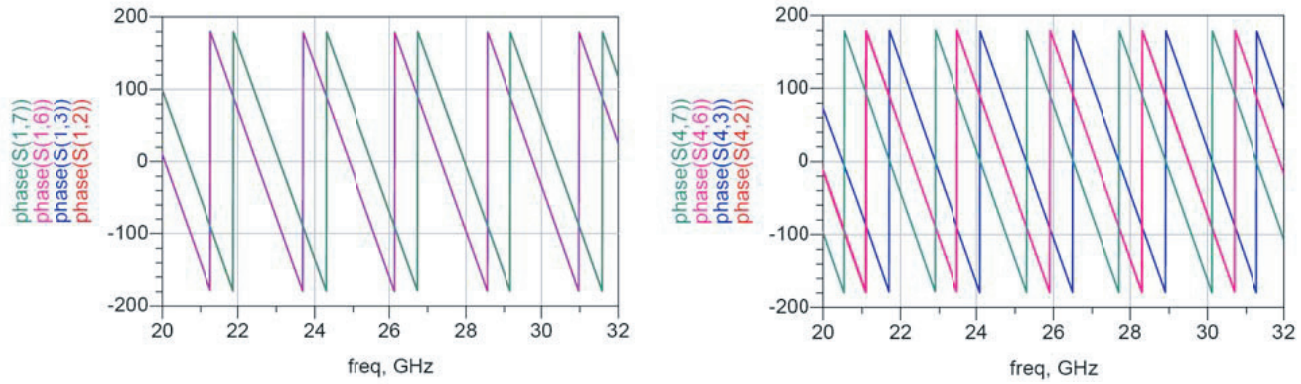

(a) (b)

Figure 19. The phase results of the transmission, reflection and isolation S parameters respect to the (a) LO port, (b) RF port.

in the RF and LO input ports, and the isolation about 25 dB between input ports. The amplitudes of transmission coefficients of the four output ports with respect to the RF and LO ports, after removing the coaxial connectors' effects, are about -6.8 and -7 dB, respectively. Fig. 19 shows the phases of these transmission coefficients, and as can be seen the phase differences are as the phase relations of S-matrix in Equation (7) over UWB frequency of 22–30 GHz, which are suitable for all UWB I/Q modulator/demodulator schemes in communication and Radar systems.

3.4. I/Q Six-Port Demodulator

Demodulation results of the six-port receiver in 21–30 GHz are presented in this section. Today MB-OFDM uses 128 narrowband channels, each channel with 4 MHz bandwidth or pulse duration of ~ 250 ns. UWB-OFDM spectrum is divided into $14 * 528$ MHz band groups, which results in 7.4 GHz bandwidth. Because in this paper instantaneous bandwidth about 9 GHz is realized, it can be used for UWB-OFDM applications in 5G new spectrum in 21–30 GHz. In each separate band of OFDM, QAM and PSK modulation schemes can be used.

So to study the proposed UWB-six-port performance in UWB-OFDM, simulations are performed using 128 various frequency points in the whole band of 21–30 GHz. Phase Shift Keying (PSK) and Quadrature Amplitude Modulation (QAM) are used to analyze phase and amplitude errors in down-

conversion. As explained before if the schematic of Fig. 16 is used for demodulation in receiver, the unwanted terms are not removed from I and Q outputs, as extracted in Equations (11), (12), and the results of QAM and QPSK are not satisfactory. Fig. 20 shows dual-ring 16-star QAM, and QPSK demodulation results using the schematic of Fig. 16 and the S-parameters of the proposed six-port structure in 21–30 GHz. The amplitude ratio of RF/LO is 0.1. As can be seen, all clusters of demodulated constellations are not well positioned at all.

If some calibrations added in receiver processing to remove the unwanted components in Equations (11), (12), the demodulation constellations will be improved to acceptable results. Fig. 21 shows dual-ring 16-star QAM, and QPSK demodulation results using the Equations (11), (12), without DC components, and the S-parameters of the proposed six-port structure in 21–30 GHz. As can be seen, all clusters of demodulated constellations are very well positioned and individualized. The resulting errors represent the difference between the actual demodulated (blue points) and the ideal symbol vectors (black points). More calibrations can be done to compensate the errors on a system; for instance, related magnitude and phase errors can be calculated for each symbol or each frequency.

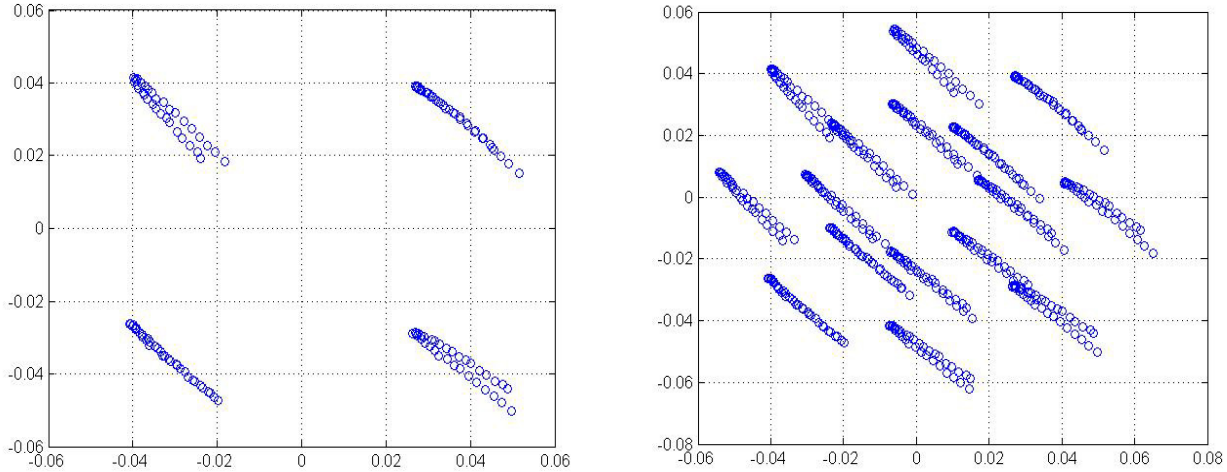

Figure 20. Demodulated results of (a) QPSK, and (b) 16QAM, before dc components removing.

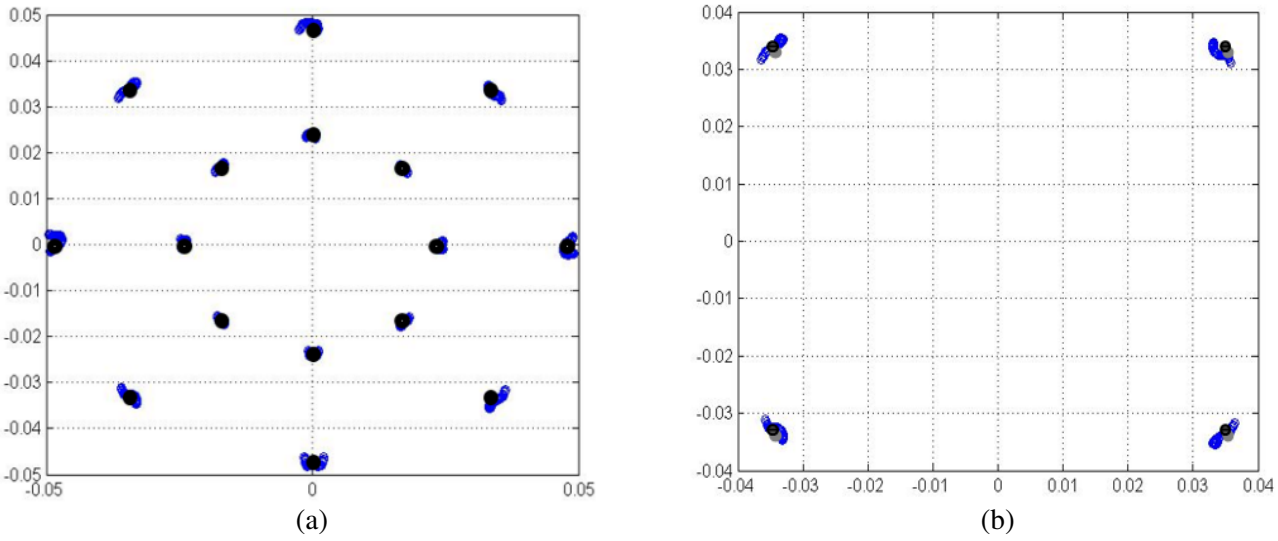

Figure 21. Demodulated results of 16QAM/QPSKM signals. (a) 16QAM. (b) QPSK.

3.5. Six-Port Modulated Ultra-Short Pulse Results

As introduced before, many applications of new 5G spectrum and CAR need ultrahigh speed connections in the range of multi-gigabit per second that can be achieved through using ultra-wide carrier bandwidths in the order of up to several hundred MHz or multi-GHz. It means that UWB-IR impulse radio works with very short signals, typically less than 0.5 ns. Therefore, UWB-IR system working with ultra-short pulse duration will be able to distinguish multipath components that are separated $\sim$ 15 cm or less. That is why UWB-IR systems are superior to narrowband or UWB-OFDM systems.

To complete the analysis of UWB-IR impulse radio with modulated ultra-high data rate signal and also to verify the new analysis of the UWB six-port structure introduced and discussed in the previous section, and also to validate the final constructed UWB six-port structure in ultra-high data rate application in 5G new spectrum of 21–30 GHz, let's inject streams of Gaussian modulated signals with ultra-high data rate up to 6.7 GHz and carrier frequency of 26 GHz, to the RF input of the final six-port structure and inject a 26 GHz CW signal to the LO port of the final six-port structure, as shown in Fig. 22.

Following the schematic of Fig. 16 and Equations (11), (12), but changing the low-pass filter (LPF) with a bandpass filter (BPF), valuable results are extracted as can be seen in Fig. 22. With this change, there is no need to calibrate the outputs of in-phase and quad phase of the six-port receiver outputs, and all effective unwanted signals are removed from I/Q outputs. Note that this new configuration

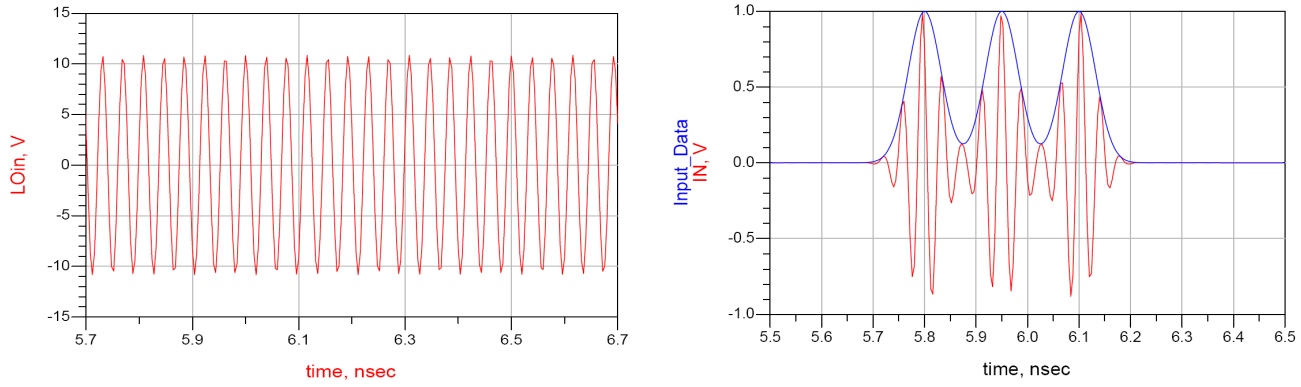

Figure 22. 26 GHz continuous Lo input signal and 6.7 Gbps Gaussian modulated RF input signal of the proposed six-port structure.

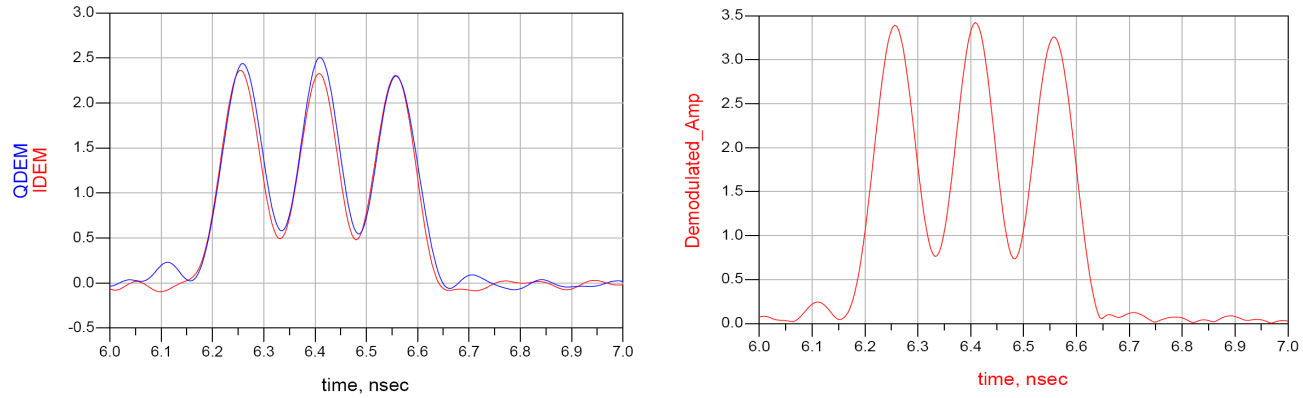

(a) (b)

Figure 23. The proposed six-port demodulated in-phase/qauad-phase (a) output signal in 45° RF phase and ((b)-sqrt($I^2 + Q^2$)) output amplitude results with 6.7 Gbps (maximum acceptable rate) Gaussian RF modulated input signal.

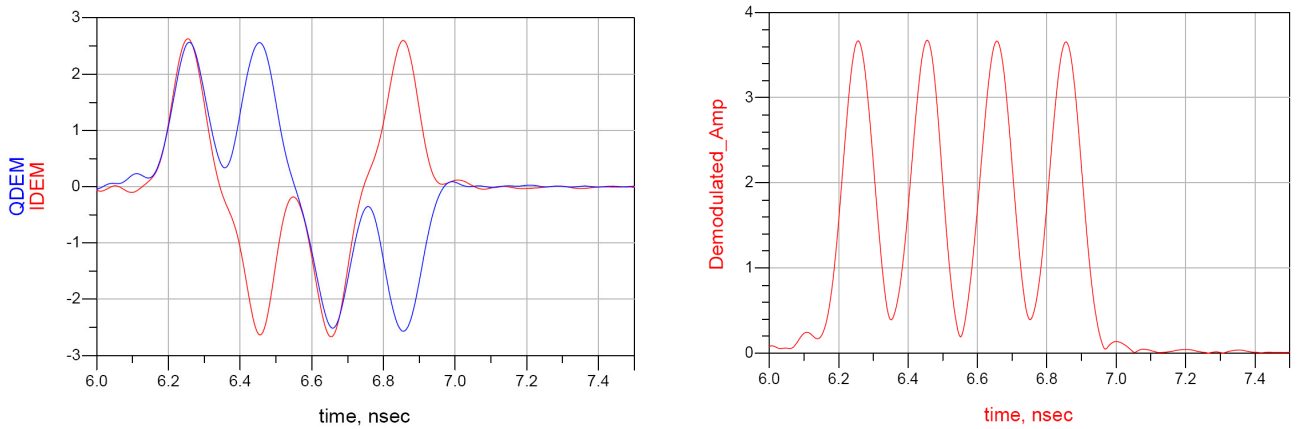

Figure 24. The proposed six-port demodulated (a) in-phase/qauad-phase and (b) output amplitude results with 5 Gbps QPSK Gaussian RF modulated input signal.

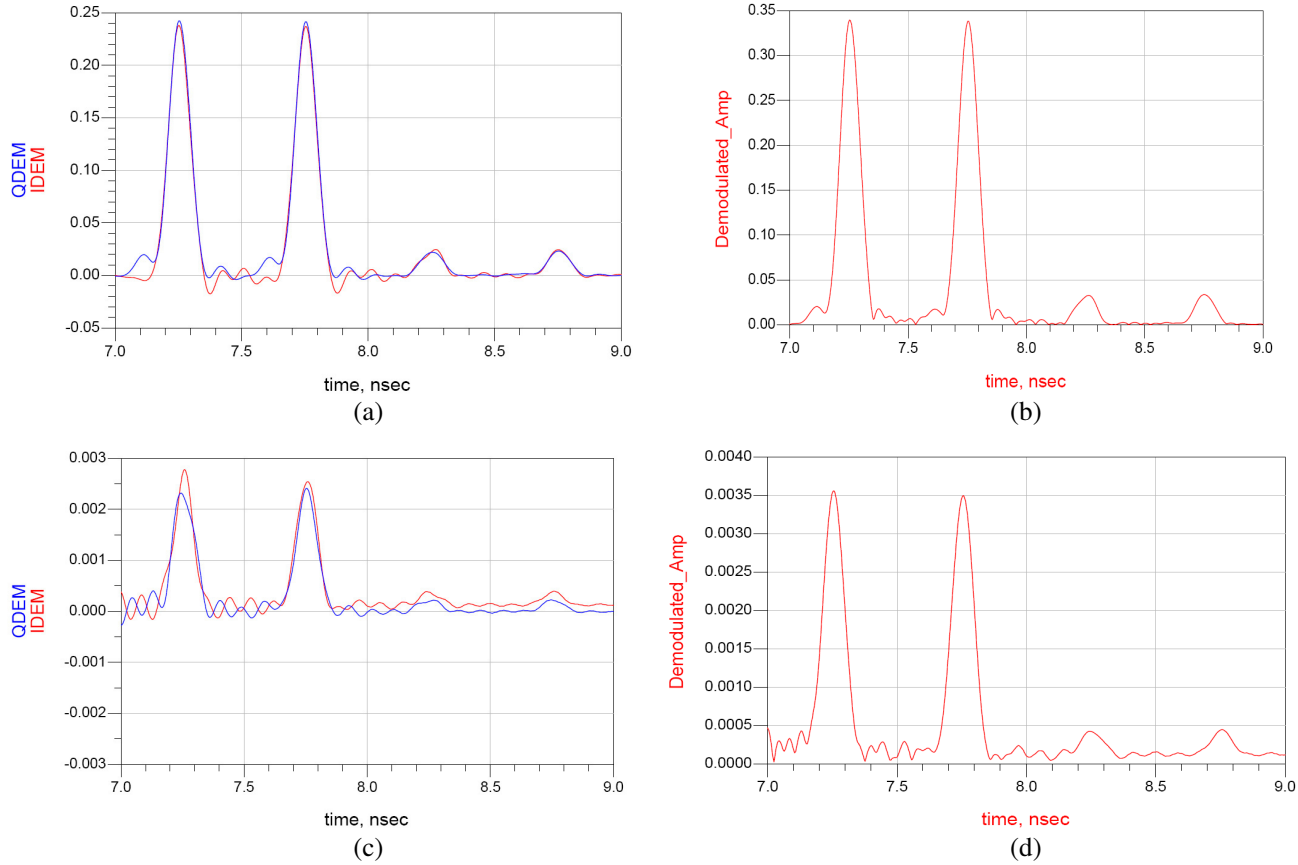

Figure 25. The proposed six-port demodulated in-phase/qauad-phase and output amplitude results with various RF to Lo input power ratio, from (a) 0, −20 dB to (d) −40, −60 dB with 5 Gbps QPSK Gaussian RF modulated input signal.

can be used only in modulated signals with the appropriate carrier, which depends on the ratio of the instantaneous band width to carrier frequency. If there is no carrier, as the standard FCC UWB signals, or if the carrier is near the instantaneous BW, the BPF cannot be used, and the unwanted signals of Equations (11), (12) must be removed by the calibration techniques in processing unit of the receiver. Also this new configuration of six-port receiver improves the dynamic range of the RF input signals up to 60 dB, as can be seen in Fig. 23. Most of the common configurations of the reported six-port receiver are sensitive to the power ratio of the RF/LO and have limited RF input dynamic range.

The proposed six-port structure can be used as Modulator/Demodulator of ultra-high data rate QPSK, 16QAM and thus UWB-OFDM and other schemes of modulating signals up to 6 GHz. As can be shown in Fig. 24, the in-phase/qauad-phase and output amplitude results of 5 Gbps QPSK Gaussian RF modulated input signal are well extracted with the six-port structure. Also shown in Fig. 25, the input dynamic range of RF signal can be at least 60 dB with remaining of ultrahigh data rate at least 5 Gbps.

4. CONCLUSIONS

Design procedure, analysis and implementation of an Ultra Wide Band (UWB) ultrahigh data rate full six-port receiver architecture up to 6.7G bps in 21–30 GHz is presented in this paper. The complete design procedure, optimization and implementation of two UWB ultra-high data rate Wilkinson power dividers/combiners and UWB ultrahigh data rate two-stage branch line couplers which are the essential components of any full six-port structure in 21–30 GHz are discussed and done to achieve the optimum performance of the final six-port structure. The final fabrication show very good results, and the average of -14 dB, -20 dB and -4.2 dB of input matching, isolation of the isolated ports, and coupling in output ports are achieved (considering 2 SMA connectors and transitions in each path) in the whole instantaneous bandwidth of 21–30 GHz. Also a new analytical model and configuration of non-ideal UWB six-port networks is presented. To complete and verify the new analysis and to validate the final constructed UWB six-port structure and its essential components in ultra-high data rate application in 5G new spectrum, the UWB-OFDM with QPSK and 16QAM demodulation schemes in its sub-bands and the UWB-IR impulse radio with modulated ultrahigh data rate signal up to 7 Gbps and in 21–30 GHz bandwidth are completely discussed. The results show that all clusters of demodulated constellations are very well positioned and individualized in whole bandwidth in all modulation schemes. Also this new design and configuration of six-port receiver improves the dynamic range of the RF input signals up to 60 dB which is valuable. During the design procedure, a useful method to choose the suitable laminate based on the time, frequency and two-dimensional Wigner-Vile distribution method is presented. Also, the coaxial to microstrip transition is considered to achieve the best results in the final six-port structure and its essential components in 21–30 GHz. A complete design in other frequency spectrum of the 5G and another complete analytical analysis of non-ideal UWB six-port structure based on all desired components are under development by the authors and will be presented in the future works.

ACKNOWLEDGMENT

The authors would like to thank "Information and Communication Technology Institute" of Isfahan University Technology for their support of fabrication and measurements.

REFERENCES

1. Ericsson White paper, "5G radio access," Uen 284 23-3204 Rev C, April 2016.
2. 4G Americas White paper, "5G spectrum recommendations," August 2016.
3. European Commission — Press release, "Commission facilitates deployment of car radar systems to boost road safety," Reference: IP/11/937, Date: 29/07/2011, http://europa.eu/rapid/press-release_IP-11-937_en.htm? Locale=en.

4. Koelpin, A., G. Vinci, B. Laemmle, D. Kissinger, and R. Weigel, "The six-port in modern society," *IEEE Microwave Magazine*, S35–S43, December 2010.
5. Nedil, M., T. A. Denidni, and H. Boutayeb, "Ultra-wideband CPW six-port circuits based on multilayer technology," *Electronics Letters*, Vol. 43, No. 23, November 2007.
6. Bialkowski, M. E., A. M. Abbosh, and N. Seman, "Compact microwave six-port vector voltmeters for ultra-wideband applications," *IEEE Transactions on Microwave Theory and Techniques*, Vol. 55, No. 10, 2216–2223, October 2007.
7. Sadler, B. M., D. Goeckel, M. L. Honig, A. J. Van Der Veen, and Z. Xu, "Introduction to the issue on performance limits of ultra-wideband systems," *IEEE Journal of Selected Topics in Signal Processing*, Vol. 1, No. 3, 337–339, October 2007.
8. Boukari, B., E. Moldovan, R. I. Cojocaru, S. Affes, K. Wu, R. G. Bosisio, and S. Ovidiu Tatu, "A 77-GHz six-port FMCW collision avoidance radar sensor with baseband analytical calibration," *Microwave and Optical Technology Letters*, Vol. 51, No. 3, March 2009, 720–725.
9. Mallat, N. K. and S. O. Tatu, "Six-port receiver in millimeter-wave systems," *International Conference on Systems, Man and Cybernetics, ISIC*, 2007.
10. Mártir, A. M. and I. M. Fernández, "Six-port junction with complete UWB band coverage in multilayer technology," *Proceedings of the 41st European Microwave Conference*, Manchester, UK, October 10–13, 2011.
11. Hammou, D., E. Moldovan, K, Wu, and S. O. Tatu, "60-GHz MHMIC six-port model analysis," *Microwave and Optical Technology Letters*, Vol. 52, No. 9, 2104–2108, September 2010.
12. Tatu, S. O., R. I. Cojocaru, and E. Moldovan, "Interferometric quadrature down-converter for 77 GHz automotive radar: Modeling and analysis," *Proceedings of the 7th European Radar Conference*, 125–128, Paris, France, September 30–October 1, 2010.
13. Hardtke, T., R. Richter, and H. J. Jentschel, "Six-port architecture based receiver for MB-OFDM UWB systems," *International Conference on Next Generation Mobile Applications, Services and Technologies, NGMAST 2007*, 2007.
14. Hammou, D., E. Moldovan, and S. O. Tatu, "Novel MHMIC millimeter wave power divider/combiner," *IEEE CCECE 2011*, Niagara Falls, Canada, 2011.
15. Hannachi, C., D. Hammou, Z. Ouardirhi, and S. O. Tatu, "Complete characterization of novel MHMICs for V-band communication systems," *Journal of Electrical and Computer Engineering*, Vol. 2013, 1–9, 2013.
16. Askari, G. H. and M. Kamarei, "Distortion analysis of UWB short pulses using time-frequency distribution," *IEEE 17th International Conference on Transparent Optical Networks (ICTON)*, Budapest, Hungary, July 2015.
17. Sadler, B. M., D. Goeckel, M. L. Honig, A. J. van der Veen, and Z. Xu, "Introduction to the issue on performance limits of ultra-wideband systems," *IEEE Journal of Selected Topics in Signal Processing*, Vol. 1, No. 3, 337–339, October 2007.
18. Fernandes, J. R., H. B. Goncalves, L. B. Oliviera, and M. M. Silva, "A pulse generator for UWB-IR based on a relaxation oscillator," *IEEE Transactions on Circuits and Systems-II, Express Briefs*, 1–5, 2008.
19. Askari, G. H., M. Kamarei, M. Shahabadi, H. Mirmohammad-Sadeghi, "Analysis, design and implementation of a broadband coaxial-to-micro strip for UWB radar," *PIERS Proceedings*, 972–977, Guangzhou, China, August 2014.
20. Pozar, D. M., *Microwave Engineering*, 4th Edition, John Wiley & Sons, Inc., 2012.
21. Raj Gopala Rao, B. V., K. Ch. Sri Kavya, K. Sarat Kumar, H. Khan, C. Manjari, Y. Sneha Priya, and G. Siva Sai Sudha, "An optimized design of wideband multi-section branch line coupler at Ka band," *International Journal of Engineering Research and Applications (IJERA)*, Vol. 2, No. 5, 655–658, September–October 2012, ISSN: 2248-9622.